Transfer Characteristics of Radial Force of Induction-type Bearingless Motors with Four-Pole Rotor Circuits

by

Akira Chiba*1, Ryoji Miyatake*1, Satoru Hara*1, and Tadashi Fukao*2

*1:Dept. of Electrical Engineering
Faculty of Science and Technology
Science University of Tokyo
2641 Yamazaki Noda Chiba Japan 278
Tel.+81(471)24-1501 Ext:3700
Fax.+81(471)25-8651

*2:Dept. of Electrical & Electronic Engineering
Tokyo Institute of Technology
2-12-1 Ookayama Meguro Tokyo Japan 152
Tel.+81(3)5734-2188
Fax.+81(3)5734-2903

Abstract: Rotor winding configurations have been proposed for induction type bearingless motors. Conventional squirrel cage rotor windings can been seen as not only 4-pole path but also 2-pole path. Thus, a part of current in 2-pole radial force windings flows into the squirrel cage rotor windings, which results in decreased radial force and serious phase-lag. Two rotor windings are proposed, which can been seen as 4-pole winding only. Secondary resistances are calculated and compared with measured values. These values are slightly high if rotor-bars are the same diameters. The phase-lags of two proposed rotors are found to be significantly smaller than those of the conventional squirrel cage rotor. Successful high speed operations are realized.

1. Introduction

High power and high speed electric machines are required for machine tools, turbo-molecular pumps, compact generators, and flywheels. Magnetic bearings have been employed in these applications [1]. However, magnetic bearings occupy considerably large area as well as a number of single phase inverters.

Bearingless motors are high speed electric machines combined with magnetic bearing functions. The compactness of bearingless motors suggests the possibility of high power and high rotational speed motors. Induction machine type bearingless motors have been studied in several countries [2-6]. A bearingless motor with 4-pole and 2-pole windings in stators is practical because these windings are differential to each other.

If a squirrel cage rotor of conventional induction motors is employed in the bearingless motors, a serious phase-lag occurs in relationships between radial force and its winding current. A phase-lead compensation in radial position controllers was proposed to realize a stable levitation of squirrel cage induction motor [5]. However, it is also possible to realize a stable levitation by modifying rotor circuits. When the 4-pole and 2-pole windings are used as motor and radial force windings, respectively, rotor circuits can be constructed to generate only 4-pole paths, so that the phase-lead compensation is unnecessary. Two rotor windings, which can be seen as only 4-pole windings, have been proposed by the authors [6]. A stable magnetic levitation has been reported. However, theoretical calculation of rotor resistances has not yet made clear. In addition, the fabricated rotors have been made of different diameters of rotor-bars, which have made comparisons difficult.

In this paper, two proposed rotors as well as a conventional squirrel cage rotor are fabricated with the same diameters of rotor-bars for easy comparisons. In addition, secondary resistances seen at motor winding terminals have been theoretically calculated. The results of the calculation show a slight increase in motor secondary resistance. These results are confirmed in experiments. The effectiveness of proposed rotors is also confirmed in experiments measuring phase-delay angles.

2. Influence of phase-lag

Bearingless motor has 4-pole motor windings and 2-pole radial force windings. Both 4-pole and 2-pole three-phase windings are wound in a stator. As shown in Fig.1 and Fig.2, two equivalent circuits can been drawn when a rotor is positioned at stator center. One is at 4-pole motor winding terminals and the other is at 2-pole radial force winding terminals. There is no mutual coupling between 4-pole and 2-pole windings. Radial force is generated with an interaction of 4-pole and 2-pole fluxes. Thus, radial force is proportional to the currents I_{mm} and I_{mb} of magnetizing inductances of 2-pole and 4-pole windings. Let us suppose that the field flux of motor is kept constant, i.e., I_{mm}= const., by motor controllers. This can be realized by field oriented controllers. On the other hand, it is very difficult to regulate I_{mb} because several frequency components are injected

into radial force winding terminals to realize stable levitation. One of these has the same frequency of motor winding currents to keep a balance with gravity force. In this case, the slip S_b shown in Fig.2 is about 50 percents because the exciting frequency of 4-pole motor windings is equal to that of 2-pole radial force windings. If secondary resistance R_{2b} of 2-pole radial force windings is low as squirrel cage windings, a part of line current I_{2s} in the 2-pole radial force windings flows into the secondary circuit. Then, a transfer function I_{mb}/I_{2s} results in a phase-lag function. Moreover, the transfer function depends on the frequency of injected current at radial force winding terminals, because the slip S_b is determined by the injected current frequency and rotor rotational speeds. The phase-lead compensation proposed in [5] was designed only for static force compensation, but not for other frequency components. This phase-lead compensator was found to be effective to a test machine with squirrel cage rotor, experimentally. However, in the principles, the compensator should be constructed for all frequency components depending on rotor rotational speeds. It is also noted that phase-lead compensation results in high gain and noisy signal conditions.

Fig.3 explains a problem in static force generation. Suppose gravity force F is applied to the shaft. Then, negative feedback loops automatically detect radial displacements and generate radial force command F_β^* as shown. The generated F_β^* in controllers has the same amplitude and is oriented to the β-axis. This is true only at zero rotational speed in the case of squirrel cage rotors. As the speed increases, the radial force command F^* is automatically generated, which amplitude is increased and direction is oriented in delay-angle of ϕ_m. This fact can be explained that the negative feedback loops are automatically compensating a phase-lag angle caused in bearingless motors. The phase-lag angle ϕ_m and the amplitude F^* increase as the rotational speed increases. Despite of the effects of negative feedback loops, the phase-lag in bearingless motors results in the decrease of phase margin of radial position control loop, which finally results in instability. In order to avoid these problems, it is very preferable to make the rotor circuit resistance R_{2b} of 2-pole radial force windings as high as possible. This can be achieved by wound rotors of induction motors.

3. Structure of proposed rotor windings

Fig.4 shows three rotor circuits for 16-slot rotors and the dimensions of secondary conductors. Fig4(a) shows a conventional squirrel cage rotor of typical induction motors. Fig4(b) shows one short circuit path of 2-phase rotor. Fig4(c) shows one short circuit for 4-phase rotor. The short circuit paths of proposed rotors are connected so that only 4-pole circuits are constructed.

The rotor in Fig.4(c) is ideal, however, it is rather complicated to construct 4 coil-end conductors. As 4 layers of coil-end conductors are constructed, the length of rotor-bars must be increased. Thus, rotor resistance R_{2m} seen at motor terminals increases.

The rotor in Fig.4(b) is mechanically simple with less coil-end conductors compared with one in Fig.4(c). However, a part of rotor shown in Fig.4(b) can be seen as squirrel cage. Thus, a few amount of current in 2-pole radial force windings flow into rotor windings. This fact results in low resistance in R_{2b} compared with the rotor in Fig.4(c). It is also understood that R_{2m} is increased compared with the squirrel cage rotor because the length of rotor-bars must be increased.

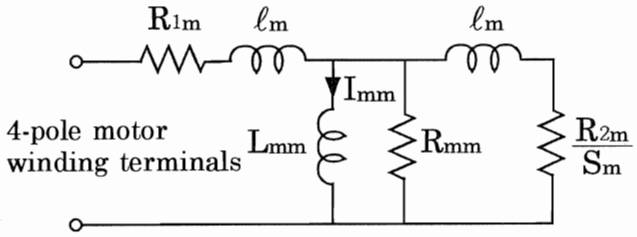

Fig.1 Equivalent circuit of 4-pole motor windings

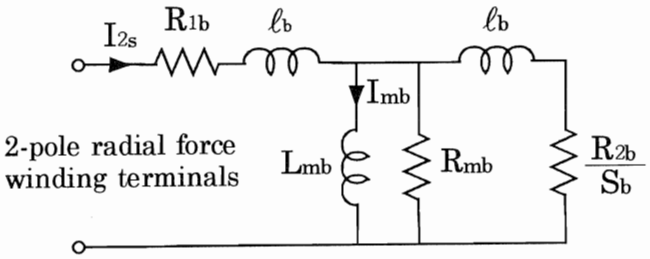

Fig.2 Equivalent circuit of 2-pole radial force windings

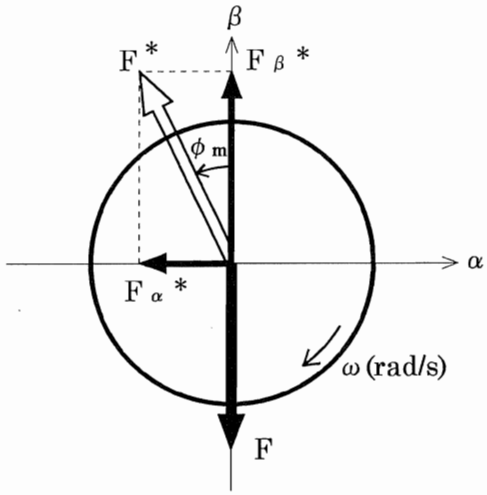

Fig.3 Influence of phase-lag

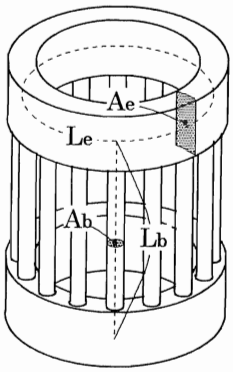

(a) Squirrel cage rotor

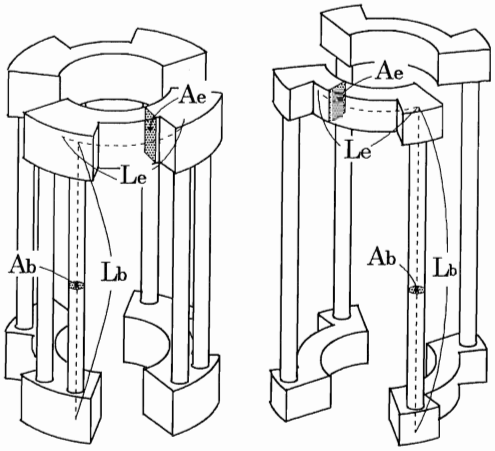

(b) Rotor 1 (c) Rotor 2

Fig.4 Structure of rotor windings

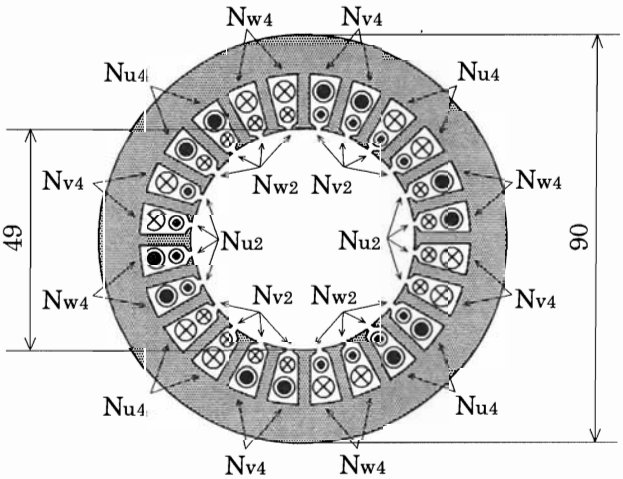

(a)Stator iron and windings

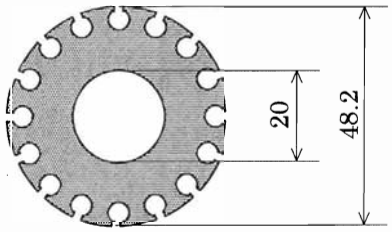

(b)Rotor iron

Fig.5 Dimension of stator and rotor

4. Calculation of secondary resistances

4.1 Dimensions

Fig.5(a) shows the dimension of stator core and windings distribution. The inside diameter of stator is 49mm. The outside diameter of stator is 90mm. Both 4-pole motor windings and 2-pole radial force windings are concentratedly wound with ϕ 0.6mm copper wires. The number of turns in 4-pole motor and 2-pole radial force windings for one phase N_{u4} and N_{u2} are 48 turns and 36 turns per one slot, respectively. Fig.5(b) shows the dimension of rotor iron core. The diameter of rotor is 48.2mm. The stack length is 30.8mm. The length of air gap is 0.4mm, when the rotor is centered.

Fig.4 also shows the dimensions of secondary conductors of three rotors. The diameter of rotor-bars is 3.6mm for all three rotors. The cross section area A_b of a rotor-bar is 10.2mm^2. The cross section area A_e of end-ring of squirrel cage rotor was designed to be wide enough, i.e., 79.3 mm^2. The cross section area A_e of coil-end of rotor1 is also wide enough, i.e., 54.0mm^2. The cross section area A_e of coil-end of rotor2 is 35.4 mm^2. The all coil-end conductors are designed to be wide enough, so that the secondary resistances are decreased. The lengths L_b of rotor-bar of squirrel cage rotor, rotor1 and rotor2 are 42.8mm, 57.5mm and 68.0mm, respectively. It is seen that thick coil-end conductors result in long rotor-bars. Thus, values of R_{2m} increase as the lengths of rotor-bars are increased. The circular length L_e of end-ring of squirrel cage rotor is 133.2mm. The circular length L_e of coil-end of rotor1 and rotor2 are 23.6mm.

4.2 Calculations of secondary resistances

In this section, the secondary resistances R_{2m} of 4-pole motor windings are calculated theoretically. The relationships between secondary resistances and physical dimensions and connections of rotor-bars are made clear. Some basic assumptions are employed. Iron loss resistance R_{1m} and leakage inductance ℓ_m are ignored. Fig.6(a) shows ideal transformer. The power factor is $\cos\theta$, thus, $I_1\cos\theta$ indicates a real power current component. The n_1 and n_2 are number of turns in primary and secondary windings. A basic relationship is,

$$n_1 I_1 \cos\theta = n_2 I_2$$

This equation shows that mmfs are the same at both terminals. Suppose that N_1 is a number of series conductors per one slot in a stator, i.e., 48T. Two slots are used for one phase of 4-pole windings. In addition, (3/2) times of mmf is generated with 3-phase windings. Thus, mmf of primary windings is,

$$2N_1 I_1 \cos\theta \times \frac{3}{2} \qquad (1)$$

Fig.7 shows the distribution of current that flows in secondary conductor. The sinusoidal current distribution is assumed. Let us define the pole pitch τ, i.e., $2\pi R/4$, where R is rotor radius. Let also define the rms current of rotor-bars as I_b. The instantaneous current value i at the position x is written as,

$$i = \sqrt{2} I_b \sin(\frac{\pi}{\tau} x)$$

Fig.8 shows that current flows in several rotors. The symmetrical current distribution suggests that the current in the rotor-bar 8 is equal to that in the rotor-bar 11. In the same manner, rotor-bars 9 and 10 carry the same value in current. Thus, mmf generated by rotor current is obtained by twice of an integral of a half pole pitch, i.e.,

$$I_2 = \left| \frac{1}{\tau/2} \int_0^{\tau/2} \frac{N_2}{p} I_b \sin(\frac{\pi}{\tau} x) dx \right| \times 2 \qquad (2)$$

where, N_2 is a number of rotor-bars, i.e., 16. The N_2/p indicates a number of rotor conductors in the pole pitch, i.e., 4. Executing the integration,

$$I_2 = \frac{N_2 I_b}{4\pi} \times 2$$

As the transformer in Fig.6 is ideal, the mmf of the primary side is equal to that of secondary side as,

$$2 N_1 I_1 \cos\theta \times \frac{3}{2} = \frac{N_2 I_b}{4\pi} \times 2 \qquad (3)$$

I_b is derived from (3) as,

$$I_b = \frac{N_1 I_1 \cos\theta}{N_2} \times 6\pi \qquad (4)$$

As shown in Fig.8, I_b seems to be distributed in three rotors, but the current path of secondary conductor is different. Thus, the copper loss W in secondary conductors should be calculated in each rotor.

(a)Squirrel cage rotor

The current of squirrel cage rotor flows as shown in Fig.8(a). The peak current of end-ring $\sqrt{2} I_r$ is a half of sum of current of pole pitch τ as

$$\sqrt{2} I_r = \left| \frac{1}{\tau/2} \int_0^{\tau/2} \frac{N_2}{p} \sqrt{2} I_b \sin(\frac{\pi}{\tau} x) dx \right| \qquad (5)$$

Executing an integration, I_r is,

$$I_r = \frac{N_2 I_b}{p\pi} \qquad (6)$$

Resistance is proportional to length of conductor and inversely proportional to cross section area of conductor. The conductivity of copper is 0.021 $[m\Omega \cdot mm^2/mm]$ at 75℃. Suppose the length and cross section area of rotor-bars and end-rings are L_b, A_b, L_e, and A_e, respectively. These values in test machines are summarized in Table.1. Then, a rotor-bar resistance R_b and an end-ring resistance R_e are,

$$R_b = 0.021 \times \frac{L_b}{A_b} \qquad (7) \qquad R_e = 0.021 \times \frac{L_e}{A_e} \qquad (8)$$

Secondary conductors in squirrel cage rotor consist of 16 rotor-bars and 2 end-ring conductors. Thus, the copper loss W in secondary conductor is shown as,

$$W = 16 R_b I_b^2 + 2 R_e I_r^2 \qquad (9)$$

Substituting (6) yields,

$$W = 2 I_b^2 (8 R_b + \frac{R_e N_2^2}{p^2 \pi^2}) \qquad (10)$$

On the contrary, W can be expressed from Fig.6(b), neglecting R_{1m}, ℓ_m and R_{mm} as,

$$W = 3 \times R_{2m} (I_1 \cos\theta)^2 \qquad (11)$$

Substituting (4) into (10), and equating (10) and (11), R_{2m} is derived as,

$$R_{2m} = \frac{24\pi^2 N_1^2}{N_2^2} (8 R_b + \frac{R_e N_2^2}{p^2 \pi^2}) \qquad (12)$$

Substituting N_1=48, N_2=16, p=4 and resistances in Table.1, R_{2m} is,

$$R_{2m} = 1.50 + 0.12 = 1.62\Omega$$

Note that R_2 is composed of rotor-bar resistance 1.50Ω and end-ring resistance 0.12Ω. The rotor-bar resistances is predominant.

(b)Rotor1

The current of rotor1 flows as shown in Fig.8(b). The current of coil-end conductors is about two times as much as I_b. Conductor dimensions and resistances are summarized in Table.1. Secondary conductors in rotor1 consist of 16 rotor-bars and 8 coil-end conductors. Thus, W is,

$$W = 16 R_b I_b^2 + 8 R_e (2 I_b)^2 = 16 R_b I_b^2 + 32 R_e I_b^2 \qquad (13)$$

Substituting (4) into (13), and equating it with (11), then R_{2m} is derived as,

$$R_{2m} = \frac{192\pi^2 N_1^2}{N_2^2} (R_b + 2 R_e) \qquad (14)$$

R_{2m} is derived from (14) as,

$$R_{2m} = 2.01 + 0.31 = 2.32\Omega$$

The resistances in rotor-bars and coil-end conductor are 2.01Ω and 0.31Ω respectively. A slight increase in R_{2m} is seen compared with squirrel cage rotor. The rotor-bar resistance 2.01Ω is mainly caused by increased length L_b of rotor-bars.

(c)Rotor2

The current of rotor2 flows as shown in Fig.8(c). The length of rotor-bar L_b and coil-end L_e as well as cross section area of conductors are summarized in Table.1. Secondary conductors in rotor2 consist of 16 rotor-bars and 16 end-ring

conductors. Thus, W is written as,

$$W = 16R_b I_b^2 + 16R_e I_b^2 \quad (15)$$

Substituting (4) into (15) and equating it with (13), then R_{2m} is derived as,

$$R_{2m} = \frac{192\pi^2 N_1^2}{N_2^2}(R_b + R_e) \quad (16)$$

R_{2m} is derived from (16) as,

$$R_{2m} = 2.39 + 0.24$$
$$= 2.63\Omega$$

The resistances in rotor-bars and coil-ends are 2.39Ω and 0.24Ω respectively. Again, a slight increase in R_{2m} is seen. It is also noted that rotor-bar resistance is predominant. Thus, an increase in rotor-bar length L_b results in an increase in R_{2m}. An increase in rotor-bar length is unavoidable in rotor1 and rotor2. However, if thickness of coil-end conductors is decreased, the rotor-bar length can be decreased. Thus, it is true that an optimization of coil-end conductor thickness realizes a decrease in R_{2m}. It is also effective to reduce R_{2m} by increasing a diameter of rotor-bars.

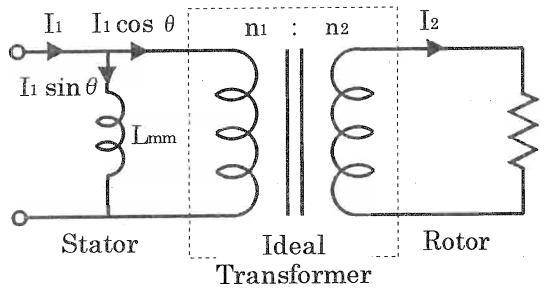

(a)Ideal transformer

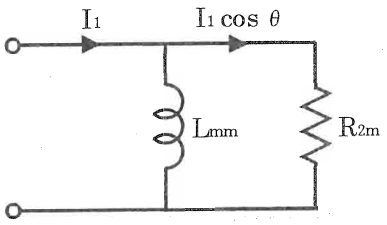

(b)Without transformer

Fig.6 Equivalent circuit of induction motor

Table.1 Dimensions of Secondary conductor

	Squirrel Cage	Rotor1 2-phase	Rotor2 4-phase
L_b(mm)	42.8	57.5	68.0
A_b(mm^2)	10.2	10.2	10.2
R_b(mΩ)	0.088	0.118	0.140
L_e(mm)	79.3	23.6	23.6
A_e(mm^2)	133.2	54.0	35.4
R_e(mΩ)	0.035	0.009	0.014
R_{2m}(Ω)	1.62	2.31	2.63

Table.2 Parameter of equivalent circuit

	R_{1m}(Ω)	ℓ_m(mH)	L_{mm}(mH)	R_{mm}(Ω)
4-pole	2.64	3.56	27.16	121.28
	R_{1b}(Ω)	ℓ_b(mH)	L_{mb}(mH)	R_{mb}(Ω)
2-pole	3.26	2.61	53.62	176.76

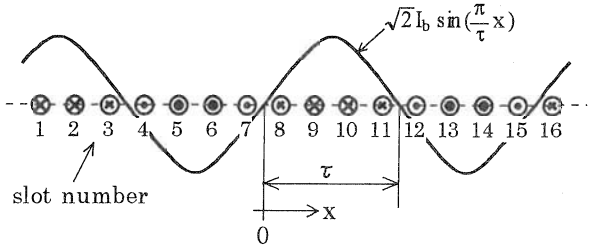

Fig.7 Current distribution in rotor-bars

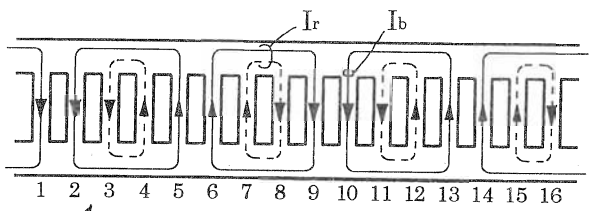

(a)Squirrel cage rotor

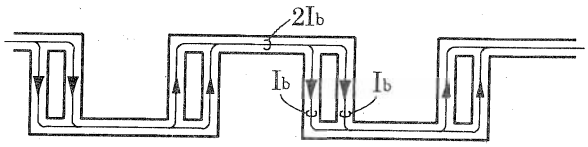

(b)Rotor1

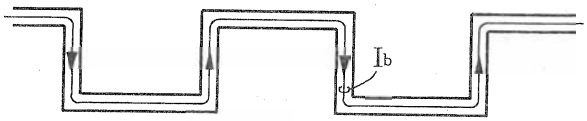

(c)Rotor2

Fig.8 Current distribution in secondary conductor

5. Measurements

5.1 Secondary resistances

In the previous section, the secondary resistances R_{2m} are theoretically derived. These R_{2m} are measured in this section to confirm the above calculation. In addition, the resistances R_{2b} are also measured. Higher is better in resistances R_{2b}. Thus, it is not possible to measure resistances R_{2m} by conventional locked rotor tests. Thus, primary winding resistances R_{1m}, R_{1b} and leakage inductances ℓ_m, ℓ_b are measured without rotor iron. Then, a rotor iron without windings is inserted in a stator. Magnetizing inductances L_{mm}, L_{mb} and iron loss resistances R_{mm}, R_{mb} are measured. Table.2 shows these measured parameters of equivalent circuits. It

is noted that magnetizing inductances L_{mm} and L_{mb} are significantly depending on exciting current level. About ±10% variations in these inductances are seen at line current of 0~2A. This fact makes it difficult to determine R_{2b}.

In order to consider the variations in L_{mb} and L_{mm}, theoretical values in power and voltage in locked rotor tests were calculated as functions of R_{2m} and R_{2b}. Fig.9 shows power and voltage variations of 4-pole motor windings terminals at unity current in locked rotor test. Fig.10 shows these variations of 2-pole radial force winding terminals. The ±10% variations are considered by the dotted lines. Table.3 shows the results of locked rotor tests. Based on the results of these locked tests, R_{2m} and R_{2b} are estimated using Fig.9 and Fig.10. For example, voltage and power are 16.24V and 8.33W in rotor1 at 2-pole winding terminals, respectively. These lines are drawn as shown in Fig.10. Considering the maximum variation of ±10% in L_{mb}, the R_{2b} is estimated to be 50 Ω.

Table.4 summarizes the measured values of secondary resistances. The secondary resistance R_{2b} of 2-pole motor windings of rotor2 is very high, so that I_{2s} does not flow into secondary circuit. Rotor2 is ideal in radial force generation. The secondary resistance R_{2b} of rotor1 is lower than that of rotor2. Thus, a few current of 2-pole radial force winding current flows into secondary resistance. In the case of squirrel cage winding, R_{2b} is as small as R_{2m}. Thus, serious problems occur in radial position control loops.

As for R_{2m}, the least resistance is realized in a squirrel cage rotor, however, slight increases can be seen in rotor1 and rotor2. The calculated values are not exactly corresponding to measured values because simplified calculation. However, the following correspondence is seen. The R_{2m} increases in squirrel cage rotor, rotor1 and rotor2. The values of rotor1 and rotor2 are increased 140~150% and 160~190% of that in squirrel cage rotor.

Table.3 Locked rotor tests

Excited Windings	Rotor Type	Current (A)	Voltage (V)	Power (W)
4-pole	(a)Squirrel Cage	1.000	4.70	4.13
4-pole	(b)Rotor1	1.001	5.50	4.71
4-pole	(c)Rotor2	1.003	5.93	5.06
4-pole	No Windings	1.003	10.18	3.26
2-pole	(a)Squirrel Cage	1.000	4.89	4.61
2-pole	(b)Rotor1	1.001	16.24	8.33
2-pole	(c)Rotor2	1.000	17.95	4.80
2-pole	No Windings	1.002	18.23	4.87

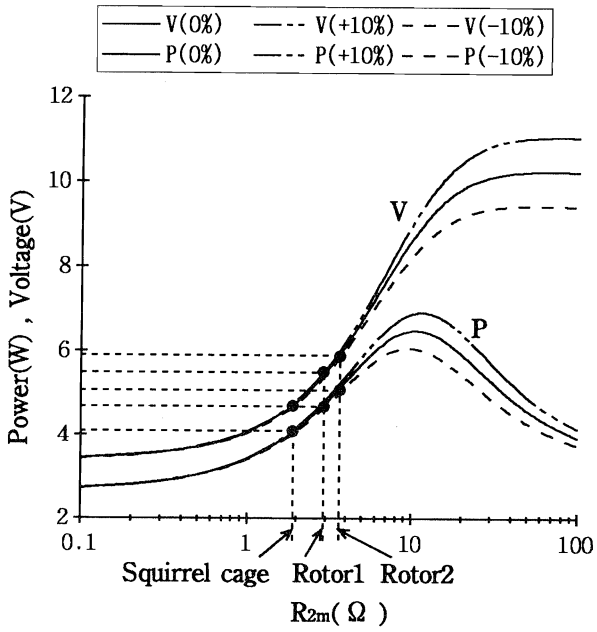

Fig.9 Power and voltage variations of 4-pole motor windings terminals at one ampere

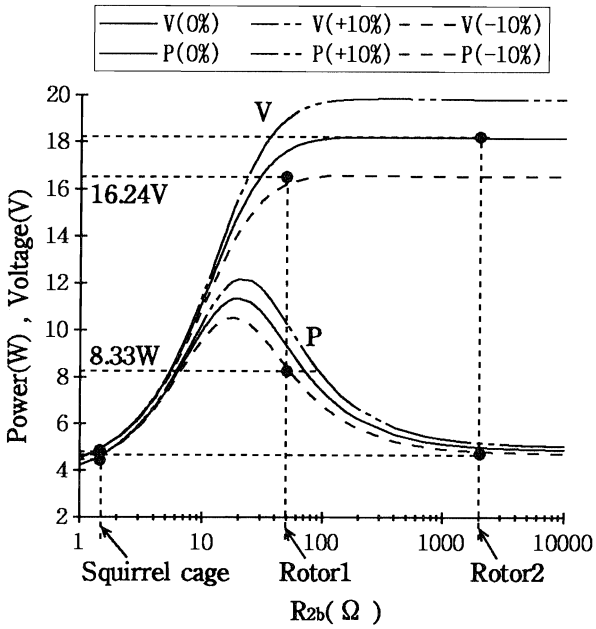

Fig.10 Power and voltage variations of 2-pole radial force winding terminals at one ampere

Table.4 Secondary resistance

Rotor Type	$R_{2m}(\Omega)$	$R_{2b}(\Omega)$
(a)Squirrel Cage	1.95	1.50
(b)Rotor1	2.95	50
(c)Rotor2	3.60	2000

5.2 Radial force

Fig.11 shows the calculated curves and the measured values in transfer characteristics between radial force and radial force winding current. The phase-lag angle can be calculated for static force from Fig.2, assuming that ω is rotor rotational speed, as,

$$\frac{I_{mb}}{I_{2s}} = \frac{\dfrac{1}{j2\omega L_{mb}}}{\dfrac{1}{j2\omega L_{mb}} + \dfrac{1}{R_{mb}} + \dfrac{1}{R_{2b}/S_b + j2\omega \ell_b}}$$

The slip S_b is almost equal to 0.5 for static force for example, gravity force. The parameters are measured as summarized in Table.2 and Table.4. The measurements of phase-delay angle are done as explained in Fig.3. The ϕ_m is measured in controller while applying static radial force to a shaft of a test machine. As shown in Fig.11, the phase-lag angle of squirrel cage rotor is 48 degrees at 5rps. Thus, the phase margin of radial position control loop becomes zero, then, it is not possible to levitate more than 5.46rps. If the rotor is forced to rotate, the shaft touches down with an emergency bearing. The phase-lag of rotor1 is 19 degrees at 60rps. The phase-lag of rotor1 is smaller than that of squirrel cage rotor. The phase-lag of rotor2 is only 3 degrees at 60rps. The phase-lags are found to be decreased with proposed rotors. Thus, it is found that these rotors can operate more than 5rps, i.e., a limited speed of squirrel cage rotor. The maximum rotational speed of 60rps(3600rpm) is mainly determined by safety reasons. It is seen that the measured values have discrepancy with the calculated curves over 25rps. The reason is that parameters of equivalent circuits have changed as the frequency is increased.

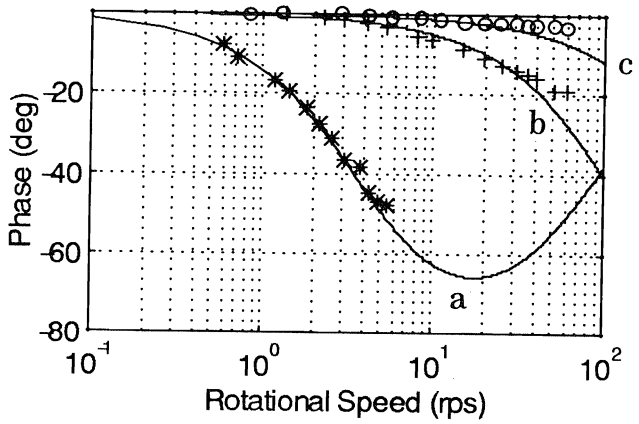

a , * : Squirrel cage rotor
b , + : Rotor1
c , ○ : Rotor2

Fig.11 Phase-lag angle

6. Conclusion

Two proposed rotors and a conventional squirrel cage rotor have been constructed. Secondary resistances R_{2m} of 4-pole motor winding terminals have been theoretically calculated and compared with measured values. The resistance is slightly increased with proposed winding configuration because of increased length of rotor-bars. However, radial force is effectively produced with few phase-delay angles. Stable levitation is realized with proposed rotor configuration.

Acknowledgment

The authors wish to thank for the technical contribution of Mr. Masao Shuto, who was a senior student in the Science University of Tokyo.

Reference

[1] Michel Dussaux "The International Application of the Active Magnetic Bearings Technology", 2nd International Symposium on Magnetic Bearings, pp.33-38

[2] R.Schob, J.Bichsel, "Vector Control of the Bearingless Motor", 4th International Symposium on Magnetic Bearings, pp.327-332

[3] Y.Okada, S.Shimura and T.Ohishi, "Horizontal Experiments on a PM Synchronus Type and Induction Type Levitated Rotating Motor", IPEC-Yokomhama'95, pp.340-345

[4] A.O.Salazar, W.Dunford, R.Stephan and E.Watanabe, "A Magnetic Bearing System using Capacitive Sensors for Position Measurement", IEEE, Trans. Mag. vol.26, no.5, pp.2541-2543, 1990

[5] S.Nomura, A.Chiba, F.Nakamura K.Ikeda T.Fukao, M.A.Rahman "A Radial Position Control of Induction type Bearingless Motor Considering Phase Delay caused by the Rotor Squirrel Cage", IEEE, PCC-Yokohama proceedings 1993, pp.439-443

[6] R.Miyatake, S.Masao, A.Chiba, T.Fukao "Comparisons with Rotor Winding Configurations of Induction Type Bearingless Motors", The 7th Symposium on Electromagnetics and Dynamics, pp.399-404 (written by Japanese)